JOURNAL OF SOLID STATE CHEMISTRY 6, 203-212 (1973)

Electrical Properties of NbO in High Magnetic Fields*,†

J. M. HONIG, W. E. WAHNSIEDLER, AND P. C. EKLUND

Purdue University, West Lafayette, Indiana 47907

Received May 22, 1972

The resistivity and Hall coefficients of polycrystalline samples, single crystals, and doped specimens of NbO_x ($0.98 \leqslant x \leqslant 1.02$) were measured in magnetic fields up to 160 kG at 4.2, 78, and 295 K. The material is found to be an excellent conductor. The results are interpreted in terms of a nearly free electron model in which holes and electrons contribute jointly to conduction processes. Orbital switching, magnetic breakdown effects, and perturbations arising from impurities are invoked to explain the observed magnetoresistance anomalies.

Introduction

Although NbO was synthesized more than 100 years ago (*1*) surprisingly little is known about its electrical properties. Meissner, Franz, and Westerhoff (*2*) studied the resistance of an uncharacterized sample as a function of temperature; they observed that the material had a positive temperature coefficient of resistivity and that it suffered a transition to the superconducting state at 1.2 K. In an unpublished thesis, Pollard (*3*) reported on a study of electrical, optical, and structural properties of a limited number of single crystal specimens; this work was briefly summarized by Pollard and Reed (*4*). In essence NbO was characterized as having all the properties anticipated for a normal metal such as silver. Roberson and Rapp (*5*), using a two-probe technique, again encountered a positive temperature coefficient of resistivity but reported values six orders of magnitude above those quoted in Refs. (*3*) and (*4*). Honig, Chandrashekhar, and Moyo (*6*) studied the resistivity of polycrystalline samples, and obtained results in substantial agreement with those of Pollard and Reed. We report here on the electrical properties of pure and doped, polycrystalline and single crystal specimens of NbO_x ($0.98 \leqslant x \leqslant 1.02$) at 4.2, 78, and 295 K in their dependence on magnetic fields up to 160 kG.

Sample Preparation and Measuring Techniques

The materials under study were synthesized in an arc plasma furnace in an atmosphere of gettered argon through the reaction $3Nb + Nb_2O_5 \rightarrow 5\ NbO$; details of this process are described elsewhere (*7*). In the earlier measurements the resulting boules were cut into rectangular parallelepipeds; a typical specimen contained between three and five large grains which could easily be perceived by the unaided eye. In later runs the buttons were transferred to a tri-arc furnace of the design by Reed and coworkers (*8*), and single crystals were grown by a technique detailed in another publication (*9*). The resulting boules generally had a square cross sectional area and were found to grow along one of the cubic axes. Sample specimens approximately $1 \times 2 \times 8$ mm could be cut on a wire saw.

All specimens were etched in CP4, washed and dried; electric leads were attached either with In solder by ultrasonic techniques or with Hg–Sn–In amalgam. The samples were mounted on an appropriate holder in a Dewar flask whose tail fitted into the central bore of an electromagnet capable of reaching fields up to 160 kG. To minimize noise problems, a voltage-to-frequency converter was used in conjunction with a scalar counter to achieve time integration of the very

* This research was supported by NSF Grant GP 8302 and GP 29221.

† The authors are all Guest Scientists, Francis Bitter National Magnet Laboratory, MIT, Cambridge, Massachusetts.

TABLE I

ELECTRICAL PROPERTIES OF NbO_x[a]

	1 2% W doped		2 1% W doped		3 $x = 0.98$		4 $x = 1.00$		5 $x = 1.019$	
	H (kG)	$R \times 10^4$ (cm^3/C)	H (kG)	$R \times 10^4$ (cm^3/C)	H (kG)	$R \times 10^4$ (cm^3/C)	H (kG)	$R \times 10^4$ (cm^3/C)	H (kG)	$R \times 10^4$ (cm^3/C)
4.2 K	34	+0.061	54	+0.502	54	−1.46	38	−1.90	38	−3.16
	68	−0.076	95	+0.134	109	−1.04	76	−3.35	76	−3.35
	102	−0.238	136	−0.016	136	−1.39	113	−4.56	113	−2.10
	136	−0.238					146	−3.92	150	−2.09
78 K	38	+1.5	54	+1.24	40	+0.41			38	−2.11
	76	+0.53	95	+0.450	95	+0.13			76	−1.67
	113	−0.077	136	+0.091	136	−0.46			113	−1.45
	150	−0.22								
295 K			41	+4.4			38	+3.19	38	+2.2
			95	+2.8			76	+2.78	76	+5.2
			135	+2.3			113	+2.58	113	+1.5
							150	+2.67	150	+1.3
	$\rho_0 \times 10^6$ ohm·cm	$\Delta\rho/\rho_0$ at 150 kG	$\rho_0 \times 10^6$ ohm·cm	$\Delta\rho/\rho_0$ at 150 kG	$\rho_0 \times 10^6$ ohm·cm	$\Delta\rho/\rho_0$ at 150 kG	$\rho_0 \times 10^6$ ohm·cm	$\Delta\rho/\rho_0$ at 150 kG	$\rho_0 \times 10^6$ ohm·cm	$\Delta\rho/\rho_0$ at 150 kG
4.2 K	0.10	7.8	0.16	4.8, 6.8	0.96	0.99	0.84	0.90	2.11	0.28
78 K	1.16	0.44	1.23	0.40	3.11	0.20			4.05	0.12
295 K	18.8	0.02	12.0		3180		10.9		10.4	

	6 $x = 1.026$		7 $x = 0.99$		8 $x = 1.00$		9 $x = 1.004$		10 $x = 1.01$	
	H (kG)	$R \times 10^4$ (cm^3/C)	H (kG)	$R \times 10^4$ (cm^3/C)	H (kG)	$R \times 10^4$ (cm^3/C)	H (kG)	$R \times 10^4$ (cm^3/C)		
4.2 K	68	−4.11	49.3	−2.1	31.8	−5.2	24.6	−0.3		
	136	−3.24	92.6	−2.3	57.3	−4.4	61.7	+0.4		
			142.0	−2.2	82.9	−5.6	98.8	−1.4		
					122.8	−5.8	135.8	−3.5		
					142.0	−5.6				
78 K	68	−2.93	76.5	−0.76	55.5	−1.2	98.8	+1.3		
	136	−2.91	140.1	−1.0	98.8	−1.5, −1.3	135.2	+1.2		
					135.8	−1.2				
					142.0	−1.2				
295 K					24.6	−0.06				
					36.9	−0.39				
					61.7	+0.084				
					67.9	−0.51, −0.44				
					98.8	−0.32				
					135.8	−0.71				
	$\rho_0 \times 10^6$ ohm·cm	$\Delta\rho/\rho_0$ at 150 kG	$\rho_0 \times 10^6$ ohm·cm	$\Delta\rho/\rho_0$ at 150 kG	$\rho_0 \times 10^6$ ohm·cm	$\Delta\rho/\rho_0$ at 150 kG	$\rho_0 \times 10^6$ ohm·cm	$\Delta\rho/\rho_0$ at 150 kG	$\rho_0 \times 10^6$ ohm·cm	$\Delta\rho/\rho_0$ at 150 kG
4.2 K	0.61	0.38	0.77	1.0	3.5	0.17 (longit.)	2.0	0.34	2.5	0.26 0.15 (longit.)
78 K	1.23	0.13	3.1	0.35	7.0	0.13	3.5	0.14	4.8	0.10 0.06 (longit.)
295 K	6.50				40	0.01	51	0.09		

[a] Samples 3–6 were polycrystalline; the remainder were single crystals.

weak signals. In resistivity measurements the current was periodically reversed to check on any spurious signals. In Hall measurements both current and magnetic field were reversed for every measurement and the appropriate average taken. A constant current source capable of providing 5 A was employed in the runs. It was repeatedly established that the sample was ohmic at these current levels. The sample was immersed in liquid helium or nitrogen for studies below room temperature; either water or the ambient air was used in measurements at 295 ± 5 K. At the conclusion of runs the sample composition was ascertained from the weight gain accompanying the reoxidation of the sample to Nb_2O_5 in air at 700°C.

Experimental Results

In Table I we summarize the Hall (R), resistivity (ρ) and magnetoresistivity (MR) data at 4.2, 78, and 295 K for two tungsten-doped and four polycrystalline samples, and for four single crystals, all of variable composition in the monophasic range (*3*) $0.98 \leqslant x \leqslant 1.02$. The magnetoresistances are tabulated at 150 kG; in several instances this required a modest extrapolation of the data.

Discussion

The following points emerge from a survey of the results:

(1) The resistivity ρ_0 at $H = 0$ usually changes by a factor of 2–3 between 4.2 and 78 K and increases by roughly one order of magnitude between 78 and 295 K. Larger resistivity changes were observed for the tungsten-doped samples. Excepting these, ρ_0 values fell in the ranges $(0.61\text{–}3.5) \times 10^{-6}$ ohm·cm at 4.2 K, $(1.2\text{–}7.0) \times 10^{-6}$ ohm·cm at 78 K, and $(6\text{–}51) \times 10^{-6}$ ohm·cm at 295 K. These bracket the values 0.67×10^{-6}, 1.4×10^{-6} and 20×10^{-6} ohm·cm cited by Pollard and Reed (*3*, *4*) for these temperatures.

The resistivities obtained with polycrystalline and single-crystal specimens were comparable. Apparently, the effect of doping and of changes in composition is more important than the state of subdivision of the samples, so long as the specimens are cut from cohesive boules.

For completeness we show in Fig. 1 a plot of ρ vs T for a single crystal $NbO_{1.00}$ specimen, based on data obtained by Chandrashekhar (*10*). It is seen that a linear variation above 100 K is superseded by a sharp changeover to a residual resistivity range dominated by impurity and disorder scattering below 50 K. The ratio $\rho(300)/\rho(4) = 18$ for this specimen.

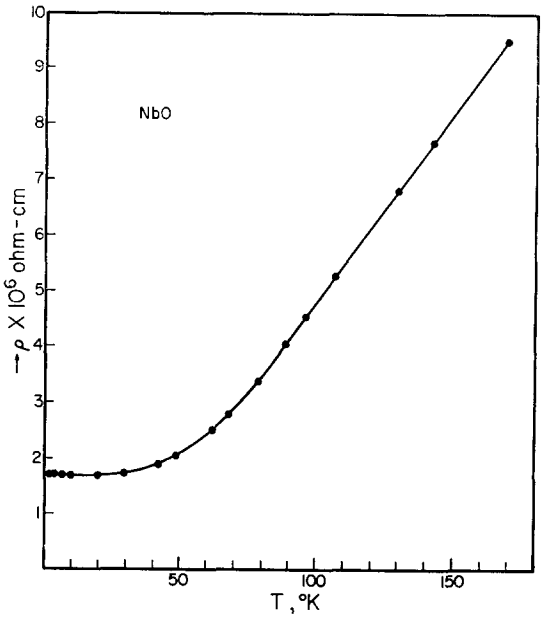

FIG. 1. Dependence of resistivity on temperature for a single-crystal $NbO_{1.00}$ specimen between 0 and 170 K. Data taken by Chandrashekhar (*10*).

(2) Samples with the lowest ρ_0 values at liquid helium temperatures exhibit the largest transverse magnetoresistivities (TMR). The effect is very marked in the tungsten-doped specimens, reaching values of $\Delta\rho/\rho_0$ up to 8 at 150 kG and 4.2 K. For the undoped specimens the TMR at 150 kG encompass the range 0.26–1 at 4.2 K, 0.11–0.35 at 78 K, and 0.01–0.09 at 295 K. Such values are orders of magnitude larger than those predicted for metals in which electrons in a single band participate in conduction (*11*, *12*). These TMR values are, however, consistent with a complex band structure, in which electrons and holes coexist, due to band overlap (*12*, *13*).

(3) At least four types of TMR curves were encountered: (A) those which show an incipient negative effect, followed by a positive upswing (cf. Fig. 2); (B) those which exhibit large values coupled with a constantly diminishing slope (cf. Fig. 3); (C) those which vary as H^2 below ~20 kG and then rise linearly with H (cf. Fig. 4); (D) and those which exhibit an initial jump in TMR (cf. Fig. 5). All TMR studies reported to date by others (*3*, *4*) and by ourselves reveal a linear or near-linear rise of the TMR with H for $H > 25$ kG. A negative contribution to the TMR has

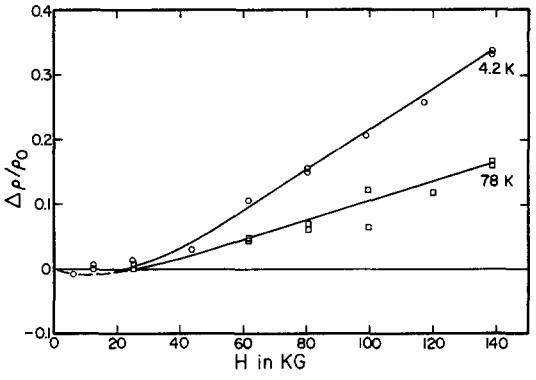

FIG. 2. Transverse magnetoresistance of $NbO_{1.004}$ single crystals at 4.2 and 78 K.

been repeatedly observed by us on a variety of samples.

These various observations cannot be explained on an elementary model. For a fixed orientation of the sample in a magnetic field H the TMR is expected (*11–14*) to vary initially as H^2. This dependence will persist indefinitely for pure intrinsic or exactly compensated materials so long as electrons can trace out open trajectories in a single average direction in reciprocal space. If the trajectories are closed or if there are significant departures from exact compensation then the TMR will saturate. The changeover from H^2 to H^0 dependence occurs for lower $\Delta\rho/\rho_0$ values at greater departures from exact compensation. However, neither the occurrence of negative TMR effects nor the linear variation of all TMR with H is predicted by the conventional theory. We will argue below that these effects arise from the joint action of magnetic breakdown, of changes in electron orbit contributions, and of impurities.

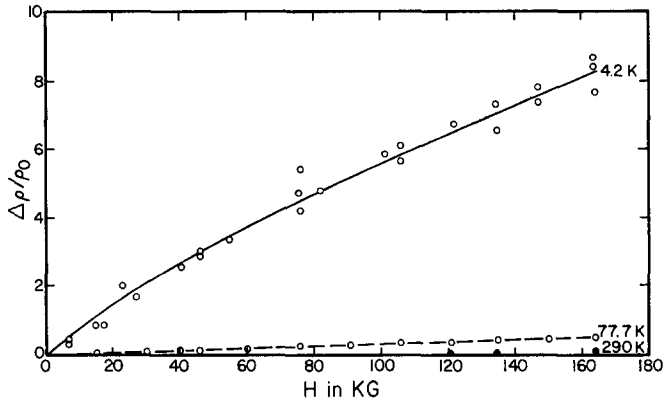

FIG. 3. Transverse magnetoresistance of a 1% tungsten-doped NbO polycrystalline specimen.

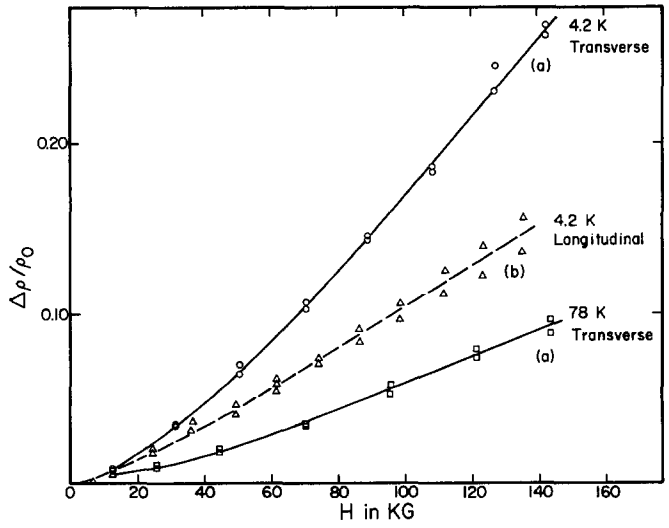

FIG. 4. Magnetoresistance of $NbO_{1.010}$: (a) transverse; (b) longitudinal.

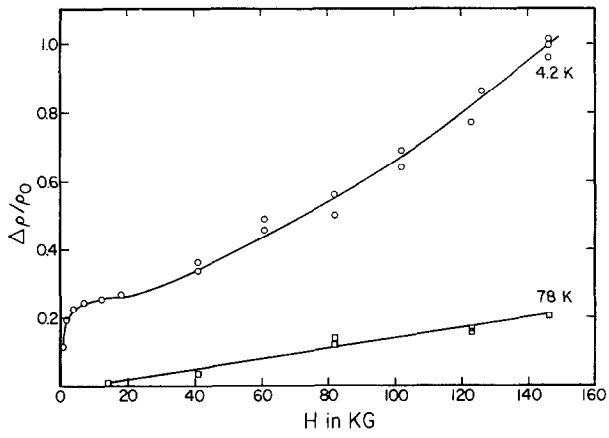

FIG. 5. Transverse magnetoresistance of $NbO_{0,98}$ polycrystalline specimen.

The possibility that the observed TMR effects are due to inhomogeneities in the samples cannot be discounted; however, for the highly metallic compound investigated here the observed effects are too large and too consistent to be ascribable solely to impurity inhomogeneities. This problem is much more serious in semiconductors with intrinsically smaller charge carrier densities. We feel that the inhomogeneity effects might distort the observed magnetoresistance anomalies, but that in their absence the MR effects would not qualitatively differ from those shown in Figs. 2–5. We recognize, however, that this matter remains to be checked out with specimens of greater purity that have been very carefully annealed.

(4) Sizeable longitudinal magnetoresistance (LMR) effects were encountered, as shown in Table I and Fig. 4b. According to standard theories (*11*, *15*), this observation rules out the presence of spherically symmetric bands in NbO.

(5) The Hall coefficients (R) ranged in magnitude between $6 \times 10^{-4} - 6 \times 10^{-6}$ cm^3/C. With rising temperature they invariably became less negative; in several instances a change in sign was observed. Samples with larger TMR effects tended to exhibit smaller Hall coefficients.

On a one-band model, the observed R values would correspond to charge carrier densities in the range 10^{22}–10^{24} cm^{-3}, as compared to a density of 4×10^{22} NbO formula units per cm^3. The above observations again force the conclusion that the band structure is complex and that more than one set of charge carriers participates in conduction.

Interpretation

We first present a qualitative argument to show that in the limit of tight binding theory NbO would be expected to exhibit metallic or semimetallic properties. Here we follow the procedures pioneered by Goodenough (*16*) in providing the qualitative counterpart of results anticipated from tight-binding analysis. The procedure is based on the NbO crystal structure shown in Fig. 6. The NbO lattice is derived from the rocksalt structure by the ordered omission of 25% of the atoms on both the cationic and anionic sublattices. Thus, each unit in the lattice is surrounded by four others of opposite polarity in a square planar arrangement, and by two vacancies in the orthogonal direction.

On the left and right of Fig. 7 we show schematically the atomic levels of Nb and of O outside

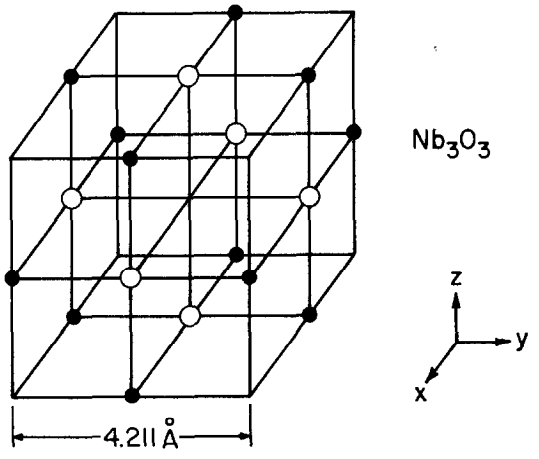

FIG. 6. Primitive unit cell for the NbO structure. Closed circles represent Nb; open circles represent O.

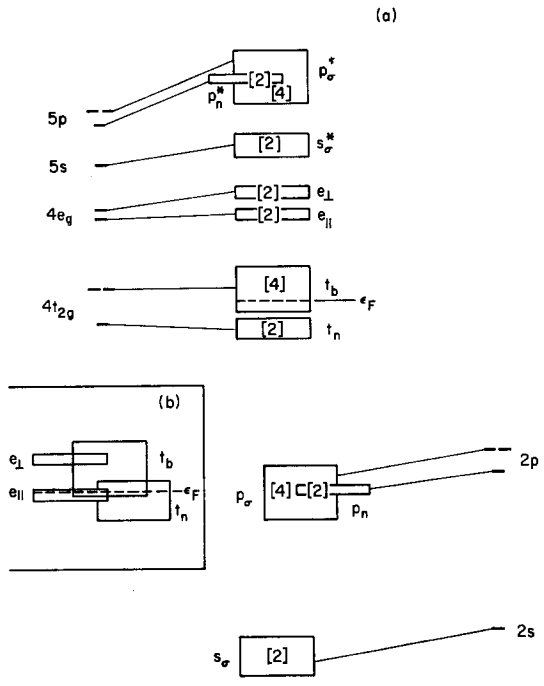

FIG. 7. Goodenough band structure scheme for NbO. Atomic-like levels subject to incipient crystal field shown on the right and left. Derived bands shown in center: (a) nonoverlapping bands; (b) overlapping bands.

filled shells, as split by the incipient crystal field of the lattice. The corresponding wave functions are oriented so as to make continuous overlap possible throughout the crystal except when incompatible symmetries are involved. As a result, each of the levels is shifted in energy and broadened into bands as shown in the center of the diagram. Those levels for which the corresponding orbitals point directly at nearest-neighbor vacancies are broadened very little; this results either in the formation of narrow bands as shown in the diagram, or else these states remain atomic in nature. The simplicity in notation should not obscure the fact that the bands are complex. For example, two of the three t_{2g} orbitals of Nb can participate in direct cation–cation overlap with corresponding orbitals on the four cations that form the next-nearest neighbors. At the same time they can engage in π-type overlap with p_π orbitals centered about the four anions that are its nearest neighbors. However, the latter are also engaged in σ bonding to e_g, s, and p_σ orbitals centered about their own nearest-neighboring cations. One thus encounters a complex interlocking band structure.

The capacities of all bands in electrons per NbO formula unit are indicated by the numbers in square brackets of Fig. 7. Ten of the eleven electrons per NbO formula unit outside completed shells fill the lower-lying s_σ, p_σ, p_n, and t_n bands. The last electron must thus be placed in the t_b band which can accommodate three more per NbO formula unit. The metallic characteristics of NbO are thus immediately rationalized, but the scheme depicted in Fig. 7(a) allows for the presence of only one set of electrons.

In the insert to the diagram we have shown an alternative disposition of the central bands which is in better accord with experimental observations. The indicated band overlap provides for the coexistence of sets of electrons and holes, as required by the data. Again, the indicated disposition of bands should not be taken literally; while we have shown a quadruple overlap of $e_\perp$, $e_\parallel$, t_b and t_n bands, the e types need not come down in energy to the extent indicated on the diagram. Only t_b–t_n-type band overlap is really required to be consistent with experimental observations, but the more complex situation of Fig. 7(b) is in better accord with the band structure scheme offered below. In any case, it is obvious that the positioning of bands on the energy scale of Fig. 7 is highly schematic in the qualitative approach taken so far. To obtain quantitative results it is necessary to resort to the tight-binding LCAO approximation scheme. Work of this nature is now in progress.

Since the Goodenough method for band construction is so highly schematic and because it rests essentially on tight-binding methodology, it was deemed desirable to attempt a more quantitative analysis, which rests on the opposite extreme, namely the nearly free electron approximation. For as metallic a material as NbO this should represent a better point of departure. In this scheme, only electrons with wave vectors near the zone edges deviate significantly from their free-particle properties. Near the zone boundaries one encounters quasi-free electron behavior as characterized by the use of effective rather than free electron masses. Therefore, most of the constant-energy surfaces in reciprocal space exhibit positive spherical curvature. This fact forms the basis of the Harrison construction technique (*17*) which allows a simple mapping of overlapping spherical Fermi surfaces that are centered about the reciprocal lattice points, from the extended zone representation into the central Brillouin zone. Failure of the Harrison technique

to account for the transition from free electron to effectively free electron behavior near the zone boundaries is reflected in the failure of the contours to bend over properly when such contours are in the vicinity of zone boundaries. Nevertheless, the technique is very useful in the understanding of band structures on a very elementary basis. We now proceed to discuss the manner in which the diagrams in Fig. 9 are obtained. For this purpose it is necessary to begin with the consideration of the reciprocal lattice to NbO.

As is seen from Fig. 6, NbO may be characterized as a simple cubic Bravais lattice with a basis. The reciprocal lattice is therefore also simple cubic; it is readily checked that the structure factor arising from the NbO basis fails to remove any of the band gaps that are encountered in the absence of this basis. The reciprocal lattice vector of length b_0 is related to the lattice parameter a_0 by $b_0 = 2\pi/a_0$, where $a_0 = 4.21$ Å. The radii k_f of the Fermi spheres satisfy the relation (*11*, *12*) $k_f = (3\pi^2 n)^{1/3}$, where n is the charge carrier density. As a simplifying approximation we shall identify n with the carrier density in partially filled bands, treating all filled bands as core states. According to Fig. 7(a) or (b) we must then choose $n = [\mathrm{NbO}]$ or $n = 3[\mathrm{NbO}]$, where [NbO] is the concentration of NbO formula units in the perfect crystal. There are three NbO units per primitive cell; accordingly, $n \approx 4.0 \times 10^{22}$ cm^{-3} or 12.0×10^{22} cm^{-3}. The corresponding Fermi radii are then 1.06×10^8 cm^{-1} and 1.53×10^8 cm^{-1}, as compared to a value of $b_0 = 1.49 \times 10^8$ cm^{-1}; thus $k_f/b_0 = 0.723$ or 1.025 respectively.

It was ascertained that with the smaller of the two radii one obtains results quite similar to those shown in Ref. (*17*). While this yields results compatible with experimental data it also requires one to consider the t_n band as a core state. Logically, it appears preferable to restrict consideration of core states to the deep lying p_σ, p_n, and s_σ bands of primarily anionic character and to others below these. For this reason we elected to choose the alternative $n = 3[\mathrm{NbO}]$.

The essentials of the three-dimensional analysis may be conveyed through the two-dimensional diagrams in Figs. 8 and 9(b). These depict respectively the Fermi contours on the plane $k_z = 0$ for the extended zone scheme and the mapping of these contours into the central Brillouin zone. Outside two filled zones, hole pockets appear in Fig. 9(b) in a third and fourth zone, and electrons sparsely occupy three additional zones.

The effects of altering the sample stoichiometry

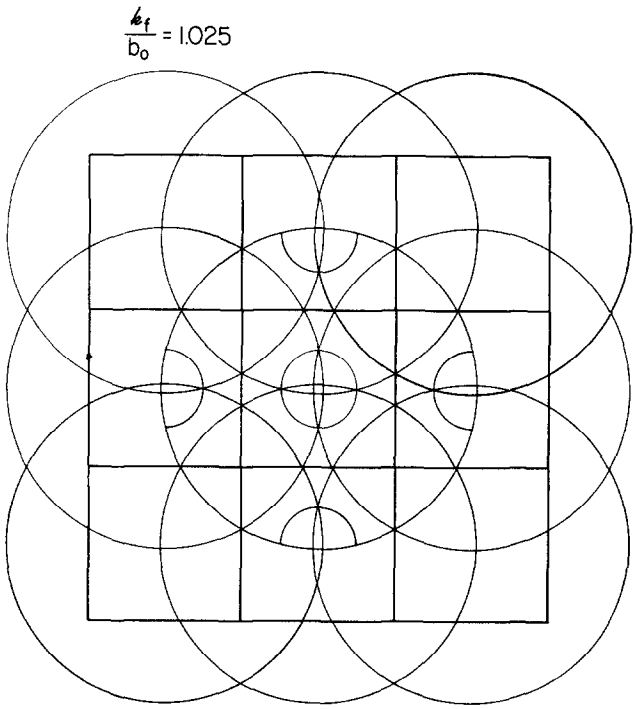

FIG. 8. Fermi contours on ⟨100⟩ planes in reciprocal space for NbO.

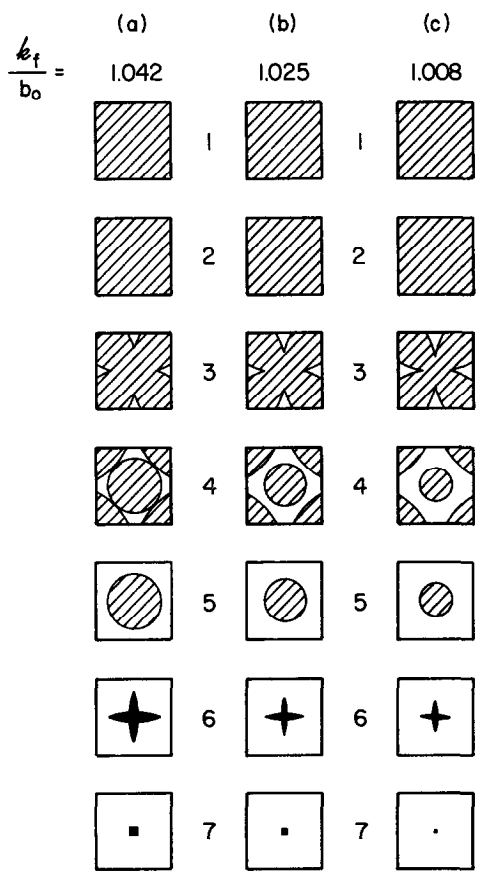

FIG. 9. Filling of various bands deriving from 3 conduction electrons per NbO formula unit, by the Harrison construction. (a) $x = 0.98$; (b) $x = 1.00$; (c) $x = 1.02$ in NbO_x.

x in NbO_x ($0.98 \leqslant x \leqslant 1.02$) is shown in Fig. 9(a) and (c), which correspond roughly to the lower and to the upper limit of monophasic stability; these results were obtained through adjustment of k_f to reflect changes in carrier density. It is seen that in proceeding to larger k_f/b_0, i.e., to lower values of x, the hole concentration increases and the electron concentration outside filled bands decreases. This fact was verified by also examining Fermi contours on various other k_z planes. The results suggest that the observed TMR should be greater at compositions closer to the lower homogeneity range. This happens to be the observed trend, though, in view of the approximations involved in the present analysis, this coincidence is probably fortuitous. Nevertheless, what does seem genuine, and is also observed in three dimensions, is the change—both in type and in concentration of carriers in several bands—as a result of small compositional changes in the compound.

Examination of Fig. 8 indicates that there is a multitude of electron and hole orbits available to charge carriers. Closed and open orbits both contribute to the trajectories of the carriers in a magnetic field. Since closed orbits give rise to saturation effects while open orbits yield magnetoresistances that vary as H^2 (*17*, *18*), a change in the number of carriers executing either type of trajectory can produce a near-linear variation of the TMR with magnetic field, of the type observed in the present experiments. We believe this to be one of the contributing factors to the experimental observations.

Equally important to our interpretation is the presence of narrow gaps resulting from the overlap of several circles, such as depicted in the center of Fig. 8. As was already noted by Pollard (*3*), the presence of such gaps may lead to the onset of magnetic breakdown effects (*14*, *17–22*), caused by the tunneling of carriers through a narrow gap under the influence of the Lorentz forces derived from the magnetic field. This effect is the analog of the Zener breakdown encountered in electric fields large enough for an interband promotion of electrons across an intervening gap. In the present case, breakdown is anticipated whenever the applied field satisfies the condition $(\hbar\omega_c \epsilon_f)^{1/2}/\epsilon_g \gtrsim 1$; here $\omega_c \equiv eH/m^*c$, ϵ_f is the Fermi energy and ϵ_g is the gap energy. The electron trajectories in low magnetic fields are limited to the intersection of the Fermi spheres with planes normal to the direction of the magnetic field (*14*); the arcs shown in Fig. 8 are examples of such trajectories. When the above condition is satisfied, the new trajectories are formed without regard to the existence of the gaps in question. In principle it is possible to switch from open to extended or closed loops or vice-versa as one passes from the low to the high magnetic field regime (*20*).

Experimentally the magnetic breakdown effect may be detected as an anomaly in the magnetoresistance; as the orbital trajectory changes, so does the dependence of the TMR on H. The details are summarized elsewhere (*24*, *25*). Specifically the TMR curves displaying an initial rapid rise, as exemplified by Fig. 5, are strongly reminiscent of those reported by Reed and Brennert (*23*) and by Stark (*24*) for zinc, where the occurrence of the breakdown has been well documented through other experimental techniques. Likewise, other types of TMR effects,

such as exemplified by Figs. 2–4, resemble those reported by Stark, Eck, and Gordon (*25*) for magnesium, where the occurrence of magnetic breakdown is again well established. Thus, in addition to the orbit-switching effect mentioned earlier, it seems reasonable to interpret our observations—notably the initial rise of Fig. 5 and the linear variation of TMR with H—in terms of magnetic breakdown effects.

A third factor contributing to the linearity of the data in Figs. 2–5 arises from the negative magnetoresistance effect. This negative component is associated with impurities through one of two mechanisms. When the contamination is sufficiently low for the impurities to exist as independent units, any magnetically active centers scatter charge carriers elastically as well as inelastically. In the latter process the carriers acquire or relinquish the energy difference corresponding to consecutive Zeeman levels of the impurity in the magnetic field. As H increases so does the Zeeman splitting, thereby decreasing the likelihood of inelastic collisions. The gradual freezing out of a scattering mechanism results in the diminution of the resistivity. Detailed theories for this effect have been published in conjunction with negative magnetoresistance effects in Ti_2O_3 (*26*). A second mechanism is encountered when impurities are so abundant as to form a band of their own, which is overlapped by the active bands of interest of the host crystal. As explained elsewhere in greater detail (*27*), the magnetic field energetically displaces the "spin-up" portion of the band relative to the "spin-down" portion; the electrons then spill over from the higher lying impurity band to lower-lying positions of the host conduction band. In so doing they now occupy band states associated with higher mobilities—hence the decline in resistivity. The electron transfer increases with rising magnetic field.

The coexistence of negative and positive contributions to the overall TMR can therefore also give rise to a range in magnetic fields where the TMR curves are linear. For, as mentioned earlier, for certain orbits the positive TMR effect is expected to undergo a smooth transition from an H^2 to an H^0 dependence. In this region the superposition of a smaller negative TMR component will then produce a resultant that should be nearly linear.

Finally, it is evident that the very small Hall coefficients and their variation with temperature are readily interpretable in terms of a rather complex band structure, for which a two-dimensional representation is shown in Fig. 9. Cardinal to the entire scheme is the coexistence of electrons and holes. If the calculations leading to Fig. 9 were taken literally, one would conclude that four sets of electrons and two sets of holes participate in the conduction process in stoichiometric NbO. The rather large changes in ρ_0 with small variations in sample composition arise in part from concomitant changes in band occupancy.

Summary

NbO is highly metallic, with a large variation in resistivity over the narrow homogeneity range in which the single phase is stable. Large longitudinal and transverse magnetoresistance effects that are sensitive to sample stoichiometry and doping are encountered, along with departures from the normal, anticipated variation of this effect with magnetic fields. A negative contribution to the magnetoresistance is observed for several samples. The Hall coefficients are very small and in some cases change sign with temperature.

The band structure for nearly free electrons resulting from the Harrison construction is indicated schematically by the two-dimensional diagrams in Fig. 9. It is evident that the overall configuration lacks spherical symmetry; this explains the sizeable longitudinal magnetoresistance effects. The free electron band model produces pockets of electrons and holes in several bands; this results in the small Hall coefficients of variable sign and in large transverse magnetoresistance effects mentioned above. The degree of occupany of the partially filled bands, and the concomitant changes in electron and hole densities, are very sensitive to small variations in sample stoichiometry or to doping. Hence, the resistivity, Hall coefficient, and magnetoresistance of NbO should likewise be sensitive to these factors; this is found to be the case. Figures 8 and 9 also show up the existence of closed and open trajectories which permit switching of orbits and magnetic breakdown effects to occur. It is postulated that these effects are partially responsible for two of the observed magnetoresistance anomalies, namely the initial jump and the linear variation of the TMR with magnetic field. Finally, the presence of impurities in NbO is believed to give rise to a negative component to

the TMR which is encountered in some of the specimens; also, it tends to extend the range over which the TMR vs H curve is linear.

Acknowledgments

The authors are greatly indebted to Professor B. Lax in providing the hospitality and to Mr. L. Rubin for providing technical assistance at the MIT Francis Bitter National Magnet Laboratory. They wish to thank Drs. T. B. Reed, E. R. Pollard, A. N. Gerritsen, and G. V. Chandrashekhar for valuable technical discussions, and to acknowledge the assistance of Dr. L. Kaufman, Mr. G. Yuochunas, Mr. L. Lonney, and Mr. A. Paladino in the preparation of sample specimens. They also wish to thank Dr. G. V. Chandrashekhar for supplying the data for Fig. 1.

References

1. H. Rose, *Pogg. Ann.* **104**, 310 (1858); **112**, 984 (1861).
2. W. Meissner, H. Franz, and H. Westerhoff, *Ann. Phys.* **17**, 593 (1933).
3. E. R. Pollard, Ph.D. Thesis, Massachusetts Institute of Technology, 1968.
4. E. R. Pollard and T. B. Reed, *Solid State Research Report*, MIT Lincoln Laboratory, No. 3, 18–20, 1969.
5. J. A. Roberson and R. A. Rapp, *J. Phys. Chem. Solids* **30**, 1119 (1969).
6. G. V. Chandrashekhar, J. Moyo, and J. M. Honig, *J. Solid State Chem.* **2**, 528 (1970).
7. T. B. Reed, E. R. Pollard, L. E. Lonney, R. E. Loehman, and J. M. Honig, *in* "Inorganic Syntheses" (A. Wold, Ed.), in press.
8. T. B. Reed, *Mater. Res. Bull.* **2**, 349 (1967).
9. J. M. Honig, G. Yuochunas, T. B. Reed, and E. R. Pollard *in* "Crystal Syntheses" (R. A. Laudise, Ed.), in press.
10. G. V. Chandrashekhar, personal communication.
11. A. H. Wilson, "The Theory of Metals", Cambridge University Press, New York (1958).
12. T. C. Harman and J. M. Honig, "Thermoelectric and Thermomagnetic Effects and Applications", Chap. 5. McGraw-Hill, New York (1967).
13. C. H. Champness, *Can. J. Phys.* **41**, 890 (1963).
14. E. Fawcett, *Advan. Phys.* **13**, 139 (1964).
15. F. J. Blatt *in* "Solid State Physics" (F. Seitz, and D. Turnbull, Eds.), Vol. 4, p. 200. Academic Press, New York (1957).
16. J. B. Goodenough, *Czech. J. Phys.* **B17**, 304 (1967); also *in* "Progress in Solid State Chemistry" (H. Reiss, Ed.), Vol. 5, p. 145. Pergamon Press, New York (1971).
17. W. A. Harrison, "Pseudo-potentials in the Theory of Metals," pp. 79 ff. Benjamin, New York (1966).
18. I. M. Lifschitz, M. Ia. Abzel', and M. I. Kaganov, *Sov. Phys. JETP* **4**, 41 (1957).
19. I. M. Lifschitz and V. G. Peschanskii, *Sov. Phys. JETP* **8**, 8756 (1959); **11**, 137 (1960).
20. E. I. Blount, *Phys. Rev.* **126**, 1636 (1962).
21. M. H. Cohen and L. Falicov, *Phys. Rev. Lett.* **7**, 231 (1961).
22. A. B. Pippard, *Proc. Roy. Soc. (London) A.* **270**, 1 (1962).
23. W. A. Reed and G. F. Brennert, *Phys. Rev.* **130**, 565 (1963).
24. R. W. Stark, *Phys. Rev.* **135**, *A*1698 (1964).
25. R. W. Stark, T. G. Eck, and W. L. Gordon, *Phys. Rev.* **133**, *A*443 (1964).
26. J. M. Honig, L. L. Van Zandt, T. B. Reed, and J. Sohn, *Phys. Rev.* **182**, 863 (1969).
27. F. T. Hedgcock and T. W. Raudorf, *Solid State Commun.* **8**, 1819 (1970).